Journal of Instrumentation

Use of a hybrid semiconductor pixel detector as a precision beam monitor at CERN accelerator facilities

Published by IOP Publishing for Sissa Medialab

Received: *January 23, 2019*
Revised: *March 3, 2019*
Accepted: *March 6, 2019*
Published: *March 18, 2019*

Use of a hybrid semiconductor pixel detector as a precision beam monitor at CERN accelerator facilities

A. Natochii,[a,b,c,1] **F. Murtas,**[c,d] **W. Scandale**[c] **and J. Alozy**[c]

[a] *Laboratoire de l'Accélérateur Lineaire (LAL), Universite Paris-Sud 11, Centre Scientifique d'Orsay, B.P. 34, Orsay Cedex, F-91898 France*
[b] *Taras Shevchenko National University of Kyiv (TSNUK), 60 Volodymyrska Street, City of Kyiv, 01033, Ukraine*
[c] *CERN, European Organization for Nuclear Research, CH-1211 Geneva 23, Switzerland*
[d] *INFN, LNF, Via Fermi 40, 00044 Frascati (Roma), Italy*

E-mail: andrii.natochii@cern.ch

Abstract: We describe the performance of the Timepix silicon detector operation at the SPS and H8 extracted beam line at CERN. Some detector calibration results and tuning will be discussed and a new cluster analysis algorithm, to reconstruct the particle hits, is described as well. We investigated the optimal acquisition setup for the Timepix device in order to use its full capabilities. A setup of 4 planes of the Timepix hybrid silicon pixel detector is tested as a hodoscope in the H8 180 GeV/c extracted pion beam, and also with a special 3 ns channeled proton bunch sequence inside the SPS accelerator. Spatial and angular distributions are measured.

Keywords: Beam-line instrumentation (beam position and profile monitors; beam-intensity monitors; bunch length monitors); Hybrid detectors; Timing detectors; Detector alignment and calibration methods (lasers, sources, particle-beams)

[1] Corresponding author.

https://doi.org/10.1088/1748-0221/14/03/P03018

2019 JINST 14 P03018

Contents

2019 JINST 14 P03018

1 Introduction

The UA9 collaboration in the last two years has installed two different types of detectors to study the channeling effect in crystals [1] in high energy particle beams at CERN accelerator facilities: Cherenkov detector and silicon pixel detector. The Cherenkov detector for proton flux measurement (CpFM) [2] has been developed by the UA9 collaboration and tested at the CERN-SPS accelerator as a proton counter. Here we evaluate the Timepix silicon quantum imager [3] as a particle counter and position sensitive beam monitor. The Timepix is the next generation of quantum imaging pixel detectors in the Medipix family, developed at CERN by the Medipix collaboration with support of the EUDET project. Details about the history and the applications of the Medipix and Timepix imagers can be found in the 10th anniversary article by Campbell [4].

Detector tuning and calibration results will be discussed. A new cluster analysis algorithm is described, which uses the time information to reconstruct the particle hits.

2 Channeling

Channeling (figure 1) is a retention of the charged high-energetic particle (with low transverse energy, an order of ~10 eV) between crystalline planes oriented within a small angle (critical angle, an order of ~10 μrad) with respect to the particle direction. A curved crystal gives a possibility to steer the particle beam in the direction of the bending.

Together with the channeling effect in the bent crystal there is another process, which conserves the total transverse energy and it is called volume reflection. It is a single reflection of the particle from the crystalline plane in opposite direction to the channeling. When the particle enters the crystal with the angle bigger then the critical angle for the channeling, the effect of the volume reflection takes place. The concurrent process to the last is a volume capture, which is the trapping of particles into the channeling regime, when the particle is close to an atomic plane loses some transverse energy.

The dechanneling is the opposite to the volume capture effect. It takes place when the particle passing the crystal in the channeling regime increasing its transverse energy in collisions with electrons (with nucleus for negatively charged particle) closer to the atomic plane, where the electron (nucleus) density is higher. Therefore, when the transverse energy exceeds some acceptance level, the particle leaves the channeling regime.

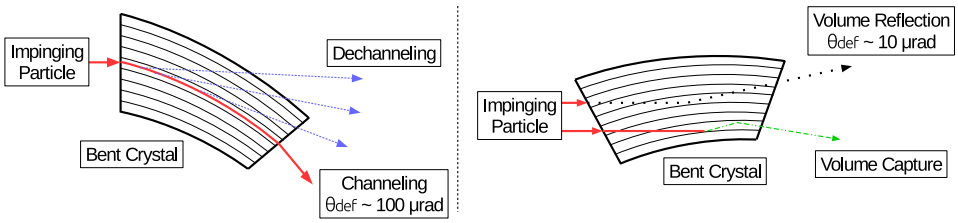

Figure 1. Schematic drawings of the charge particle interaction with a bent crystal. Channeling — red solid line, dechanneling — blue dashed line, volume reflection — black dotted line, volume capture — green dot-dashed line, while θ_{def} is the particle deflection angle due to the channeling or volume reflection processes.

3 Detector overview

3.1 Hardware

Timepix (figure 2) is a quantum imaging pixel detector of area ~ 2 cm^2, consisting of a monolithic silicon pixelated matrix of 256×256 sensitive elements, each 55×55 μm^2 and 300 μm thick, which is soldered together by 65536 metal bumps to a matching CMOS read-out chip with identical dimensions. Each pixel is a rectifying Si diode, with its volume depleted from free charge carriers by the application of a reverse bias voltage, typically 20 V–100 V, so that charge generated by an incident radiation quantum can be collected and measured. Detailed information about the charge generation and collection in a pixel is also given in [5]. Each pixel is connected to a signal processing chain of charge-sensitive preamplifier, discriminator and digital counter (14-bit, 11810 counts). Only if the signal exceeds the discriminator threshold value, a 'hit' is recorded by the

2019 JINST 14 P03018

pixel, and then the signal is processed as indicated below. The innovative feature of the pixels in the Timepix chip is the use of the threshold in combination with a MHz clock that is distributed to all pixels. The pixel can record a timetag for the moment that a signal passes the threshold in one direction: up, or the other: down. This allows to count the number of clock-pulses while discharging the signal charge via the amplifier feedback, and offers a measure of the signal amplitude, as it was proposed in 1948 by Wilkinson [6].

The readout chip further contains the Digital-to-Analog DAC power regulators, programmable parameter tuning and I/O drivers. The on-pixel threshold adjustment has 4 bits, so that a natural dispersion of the threshold values between the pixels can be precisely equalized to achieve a minimum operating threshold for all pixels of ~600 electrons [7]. This results in practically noise-free data.

The full matrix can be reset, and by opening the global shutter it is switched to exposure for a programmable period, ranging from µs to hours. After the shutter has closed again, the data from all pixels are sequentially transferred off-chip, and these represent one image 'frame'.

The Timepix pixel matrix can work in one of three modes:

- Medipix mode — Counter counts the incoming particles, which have generated an above-threshold signal.
- Time of Arrival (ToA) mode — The counter receives clock pulses (e.g. at 5 MHz) and measures the time interval, starting from the opening of the shutter until the arrival of the first signal from an incident quantum above threshold. Then the clocking is stopped for this pixel, so that only the time for the first impinging particle can be recorded.
- Time over Threshold (ToT) mode — In a similar way, the counter receives clock pulses, but these are enabled only as long as there is a signal above threshold, which is similar to the Wilkinson type ADC. This measurement provides the amplitude of the particle energy released in the pixel, and signals from successive quanta during the exposure are summed.

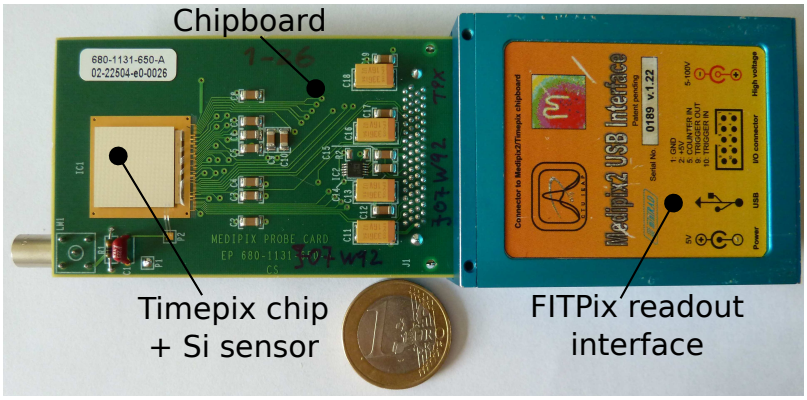

Figure 2. Timepix detector.

For communication and data transferring between Timepix and user's PC there is a FITPix [8] (fast interface for Timepix pixel detector) interface based on the FPGA circuit to achieve the high data frame-rate. It supports the serial readout through a USB 2.0 connection with a frame rate up to 90 frames/s.

2019 JINST 14 P03018

3.2 Software

The Pixelman [9] software package developed in Prague University is designed to readout the chip. The package has a very flexible modular architecture, that can be extended by software plugins (i.e. additional software that extends functionality). In our project we used two ways to communicate and control detector: (1) Pixelman Graphical User Interface (GUI) (allows to visualize the acquired frames and to write data into the text files); (2) Python scripting plugin (gives a possibility to integrate Pixelman libraries inside other data acquisition (DAQ) systems).

3.3 Equalization

Due to natural contradictions, which appear during manufacturing, some parameters of identical Timepix pixels can be different. Usually, the common value of the threshold is varying from pixel to pixel. To take into account this effect Pixelman has a function Equalization to adjust the level of the threshold for each individual pixel using a Noise Floor Equalization method [10]. After this procedure a common threshold can be applied to all pixels for the electronic noise suppression. As consequence typically no pixels is fired if there is no particle impinging on the silicon sensor.

Figure 3 illustrates the Pixelman window with an example of the threshold equalisation results. For a 100 V bias applied, the centroid is at 354.5, while the standard deviation is 1.02.

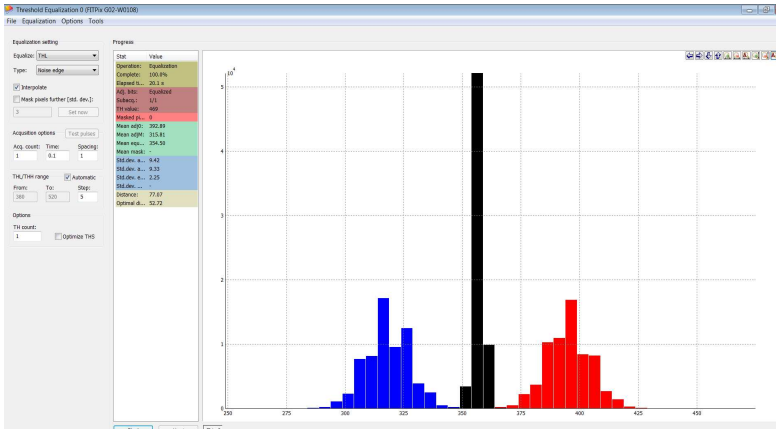

Figure 3. Typical results of the Timepix threshold equalization from the Pixelman interface.

3.4 DAQ settings

Before any detector operation, a set of the Timepix parameters has to be applied: discriminator threshold value (THL) received from the equalization function, value of the bias voltage (the capacitance of each sensor pixel depends on the applied bias voltage which affects depth of depleted zone), Ikrum (The parameter controls a discharging current in the preamplifier, i.e. the slope of a falling edge of the pulse), number of frames, time of each frame, acquisition mode (Medipix, ToA, ToT), trigger type, frequency of the measurement Clock ($\leq$96 MHz). The internal clock can be set to define the time granularity of the measurements; the maximum count of 11810 for each register attached to each pixel limits the performances of the readout. For example, for 48 MHz clock

2019 JINST 14 P03018

(~20.83 ns) in ToA mode the maximum frame duration cannot exceed $11810 \times 20.83\ ns = 246\ \mu s$. Similarly for a clock of 0.48 MHz, the time measurements up to 24 ms can be performed.

4 Experimental setup

Timepix detector has been tested inside the SPS proton accelerator beam pipe and at H8 the SPS extracted proton/pion beam line in the North Area.

4.1 H8 extracted beam line

For the bent crystal characterization before the installation in the SPS or LHC accelerators the UA9 collaboration performs measurements at the H8 SPS extracted beam line, using a dedicated tracker to successive reconstruct the track of each particle. The telescope consists of two arms (of 10 m each) of detection planes in order to reconstruct the tracks of the incoming and outgoing particles to the crystal which is located in between. The detailed description of the CMS-like tracker [11] and the standard UA9 setup at the H8 beam line is described elsewhere [12].

In 2016 and 2017 the Timepix detector was located 50 m downstream the crystal position. The usual particle beam of pions 180 GeV/c with an intensity of 10^5 particles/sec has an asymmetrical shape (figure 4) in horizontal and vertical directions with the following parameters: $RMS_X \simeq 2.3\ mm$, $RMS_Y \simeq 2.5\ mm$, $\sigma_{\theta_X} \simeq 34.6$ µrad, $\sigma_{\theta_Y} \simeq 42.8$ µrad, where RMS means a root mean square of the distribution, and σ is a standard deviation. The extraction period of the SPS to the North Area is around 40 sec with the spill duration of ~4.8 sec.

4.2 SPS

The UA9 experiment is installed in the Long Straight Section 5 of the SPS accelerator [13]. The Timepix detector was placed in the Roman Pot 1 (internal side of the accelerator ring) and Roman Pot 3 on both sides. During the dedicated machine development (MD) period at SPS, the accelerator was operated in a coasting mode with a 270 GeV/c proton beam, made of one single bunch 3 ns long, that at the start of the fill contained about 10^{11} protons. The detailed description of the operational procedure during the MD can be found in [14]. Inserting and orienting the crystal inside the beam halo a channeled beam is produced with an angle of 50–200 µrad with respect to the main beam. This secondary beam can be then quantitatively measured with the Timepix installed in the Roman Pot 1 and 3. Depending on the crystal position with respect to the beam core ($\sigma_X \simeq 0.6\ mm$), in stationary condition the number of particles from the halo reaching the edge of the crystal is varying from few to hundreds protons at every turn (23 μs).

The acquisition of each pixel matrix of the detectors is performed through an optical link in USB 2.0 protocol using a unique PC connected to each FITPixes. Figure 5 shows the scheme of the data transferring. Using a python script the data frame by frame (fired pixel coordinates and number of counts) is transferred each minute to a new data file to the CERN-DFS storage. With a BASH script running on the user PC a quasi-online analysis can be performed producing about each minute a suitable information for the MD: analyzed data is converted into the beam images and profiles, and saved on the user PC. Thus we were able to have the image of the detector frame almost immediately (the delays came only from the USB/Ethernet/Optical connection speed limits), which is the most important information needed during the MD.

2019 JINST 14 P03018

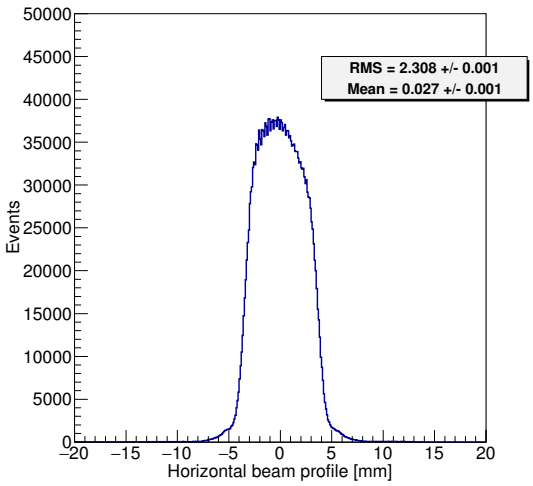

(a) Horizontal beam profile.

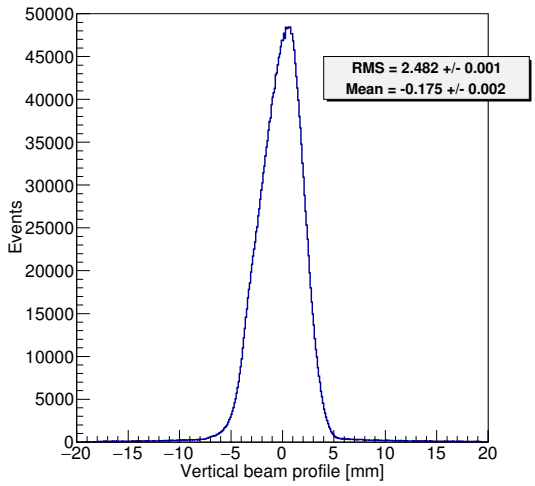

(b) Vertical beam profile.

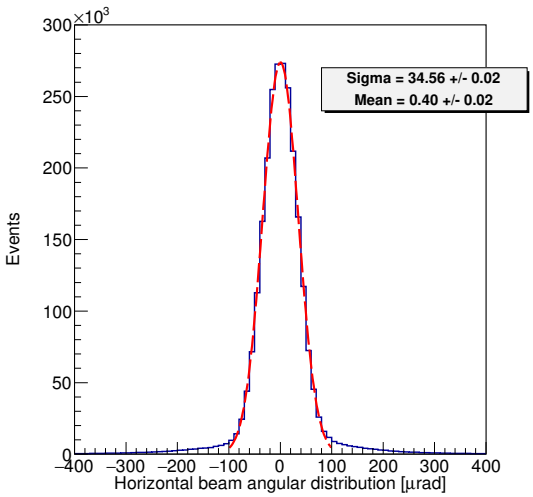

(c) Horizontal beam angular distribution.

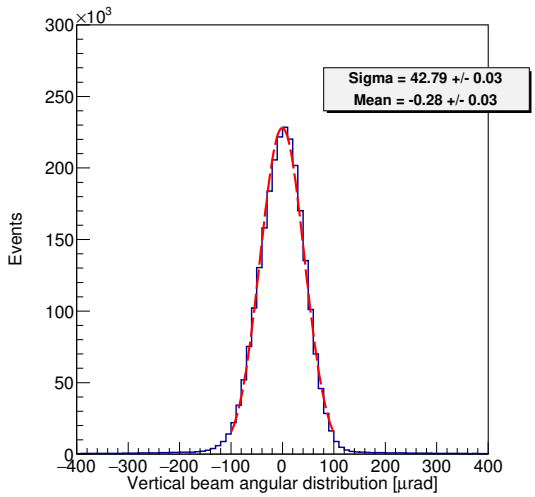

(d) Vertical beam angular distribution.

Figure 4. Typical spatial and angular particle beam distributions for the same number of incoming particles. The data is produced by the H8 beam telescope consists of Si microstrip detectors. Red dashed line is a Gaussian fit of the angular distributions.

5 Timepix operation

To provide the highest efficiency of the particle detection (sensibility to the incoming particle), it is important to apply the optimal value of the bias voltage. Under influence of the bias voltage the charge carries travel toward different electrodes. The detector used in the UA9 experiment is set to collect holes, i.e. the pixels have positive polarity.

In 2016 a test with 3.68 MBq Sr-Y beta-source has been done to evaluate the optimal value of the bias voltage. Figure 6a shows the scheme of the experimental setup. The radioactive source was

2019 JINST 14 P03018

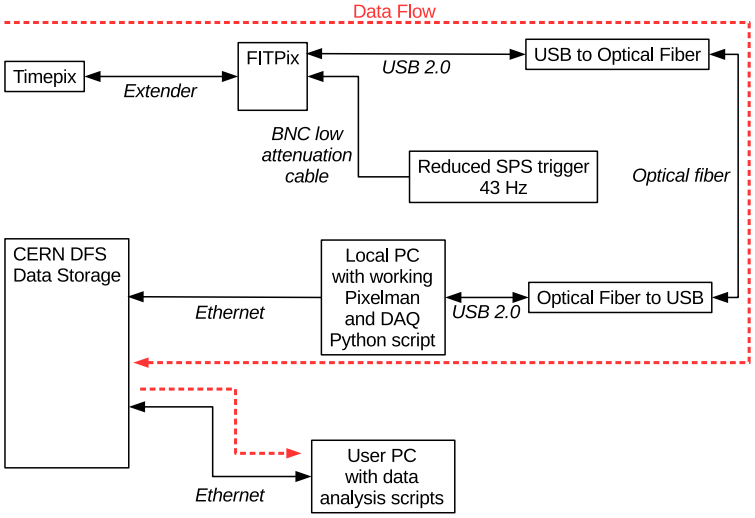

Figure 5. Timepix data acquisition network. Red dashed line indicates data flow direction.

(a) The Sr-Y source in front of the Timepix detector.

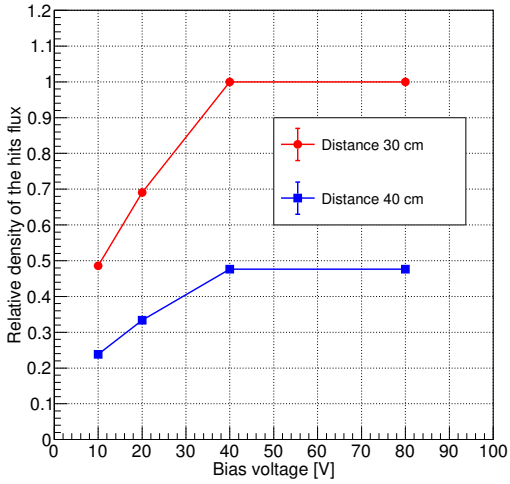

(b) The dependency between the total number of hits and applied bias voltage for different distances between the source and detector. The relative error of the values is less than 1%.

Figure 6. Detector efficiency measurements.

2019 JINST 14 P03018

placed in front of the Timepix detector. Varying the distance between the source and the detector we measured the dependency between number of the total hits and different applied bias voltage. Assuming that the flux of the particles from the source is constant during the measurements we reach the full efficiency with a bias of 40 V with silicon thickness of 300 µm (figure 6b)).

During 2017 and 2018 the Timepix detectors were operating during the SPS MDs and the H8 test-beams. At H8 beam line, the Timepix detector has been inserted in the main beam to measure the beam profile and the flux of the particles (figure 8a). While at SPS, the main goal of the detector is to characterize the deflected by the bent crystal beam (figure 7). Therefore, the Timepix sensor has been placed in such a way to intercept the channeled protons and to measure their flux at a given position along the circulating beam (figure 8b).

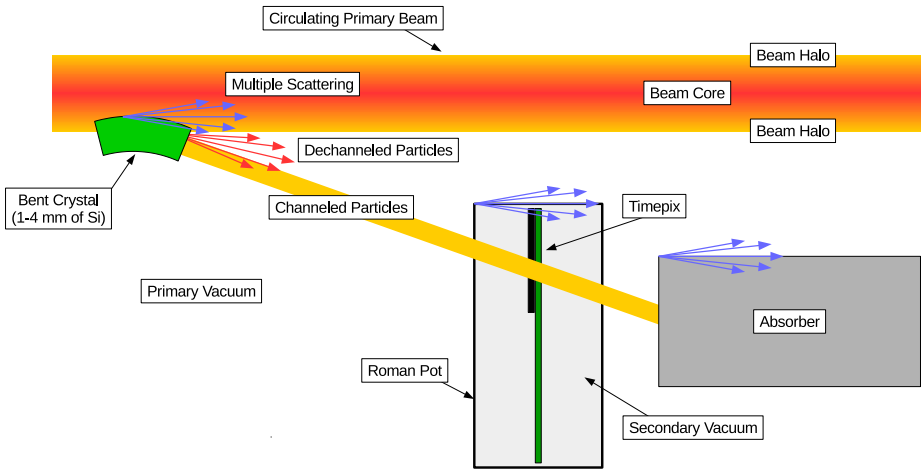

Figure 7. Conceptual sketch of the UA9 experiment with Timepix detector at the SPS accelerator. A bent crystal, inserted in the halo of the primary beam, deflects particles, while the Timepix detector, placed inside a Roman Pot cadge, intercepts the channeled beam before it will be captured by an absorber.

Figure 9 shows the time particle distribution with the SPS periodicity (43 kHz or 23 μs); where we can see 11 turns of the machine in a time window of 246 μs (Timepix in ToA mode with 48 MHz clock). With a clock set at 4.8 MHz 110 turns can be measured without dead time.

Due to the high flux of the particles at SPS we have to define the maximum acquisition time window for each frame. We collected data putting the Timepix into the channeled beam and plotting the total number of pixels (figure 10b, Y axis), which ToA is inside specified time range (figure 10b, X axis). For example (figure 10b yellow rectangle), there are about 3800 pixels with a ToA less than 10 ms. For the case without clusters overlapping the dependency should be a straight line. Otherwise we should obtain a saturation behavior. From figure 10b we can see that starting from about 0.3 ms the behavior becomes to be not linear. Thus, for the further analysis we decided to put the cut for the ToA of 0.246 ms with 48 MHz clock.

2019 JINST 14 P03018

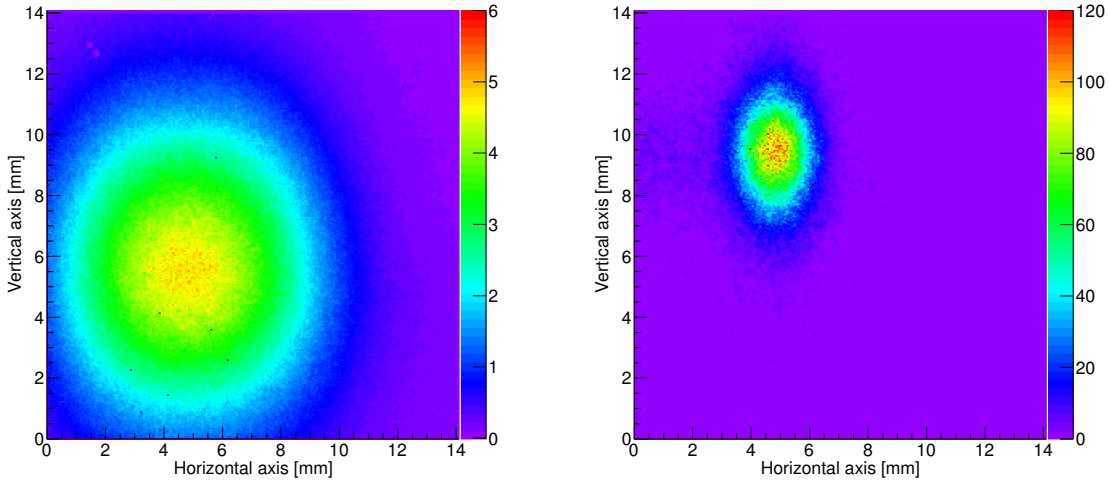

(a) The image of the pion 180 GeV/c beam in the H8 beam line.

(b) The image of the proton 270 GeV/c beam at SPS, deflected by the crystal, measured by the Timepix placed in the Roman Pot 1. The horizontal axis corresponds to the relative position of the edge of the sensor along the radial direction in the machine horizontal plane.

Figure 8. The image of the beam integrated within 1 second in the Medipix mode with 48 MHz Clock. In color (Z axis) is indicated the number of hits in each pixel per 1 second.

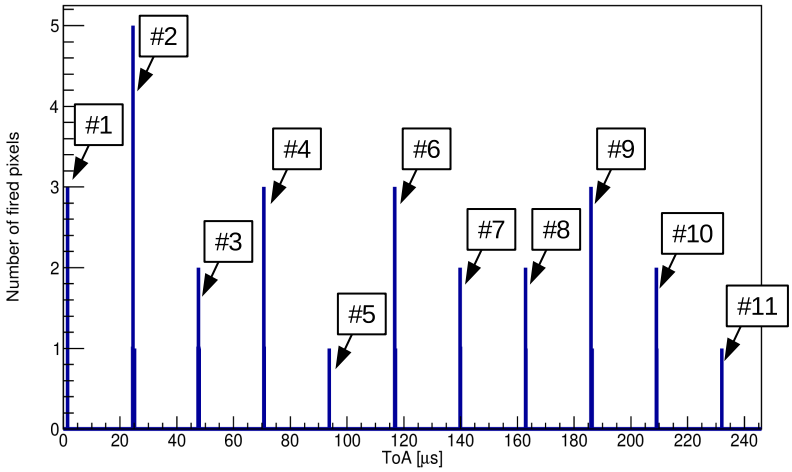

Figure 9. Distribution of the ToA for each fired pixel within one single frame of 246 μs (48 MHz clock). The distance between peaks is the period of the circulating beam in SPS equal to 23 μs. One bin of the histogram corresponds to 20.83 ns.

2019 JINST 14 P03018

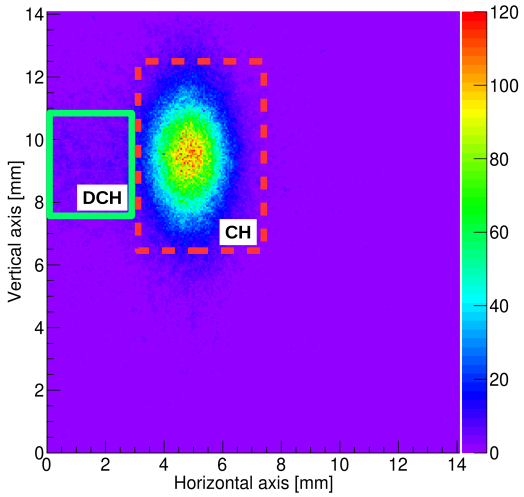

(a) Integrated image of the beam. Red dashed line — channeling (CH) region, green solid line — dechanneling region. In color (Z axis) is indicated the number of hits in each pixel per 1 second.

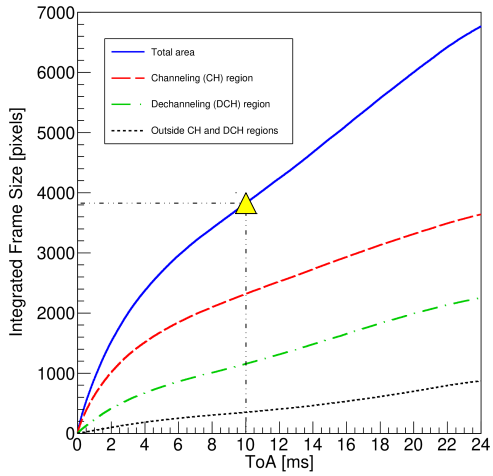

(b) Integrated number of the fired pixels as a function of the ToA. Clock is 0.48 MHz, acquisition time window is 0.0246 s. Blue solid line — total area of the sensor, red dashed line — channeling region, green dot dash line — dechanneling region, black dotted line — all others. A yellow triangle is an example point, in which there are 3800 pixels with a ToA less than 10 ms.

Figure 10. Saturation of the particle counting in the ToA mode for SPS data.

6 Results and cluster analysis improvements

For analysis of the 2016 data we used the standard Cluster Analysis [15] (CA) to identify the particle type. With this CA the cluster is recognized as the region of the fired neighbour pixels, which brings rapidly to a saturation of the particle counting caused by clusters overlapping. To solve this problem we decided to write a New (Improved) Cluster Analysis to use the information about the time of arrival in each pixel.

The time distribution of the signal arrival time in a cluster exhibits a Gaussian with 60 ns of the standard deviation (figure 11a), compatible with the drift time of the holes inside the silicon sensor with 0.3 mm thickness for 40 V of bias voltage [16]. Figure 11b shows how the time difference inside each cluster behaves with cluster size.

Therefore, the algorithm for the new cluster analysis in ToA mode consists of the following steps:

1. Applying a cut of 200 ns (i.e. $\pm 3\sigma$ for 48 MHz clock) in a time difference between pixels, we split a given frame into several subframes, where all pixels will be within this time window.

2. For each subframe, we apply the standard cluster analysis, where a single cluster is defined as a region of the fired neighbour pixels.

With a new cluster analysis algorithm in 2017 we avoided the saturation of the particle counting in the ToA mode and increase the maximum number of incoming particles per frame by factor 3

2019 JINST 14 P03018

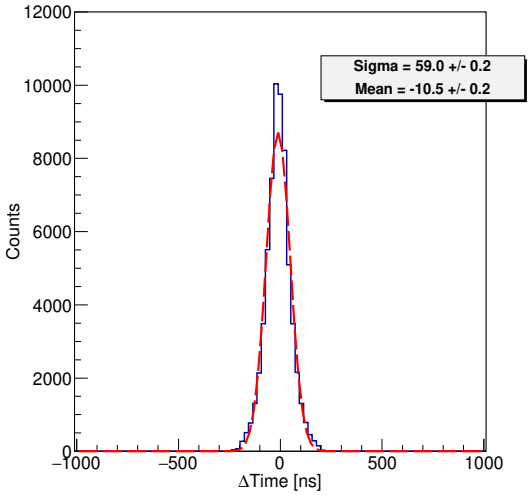

(a) Time difference of the pixels inside each cluster.

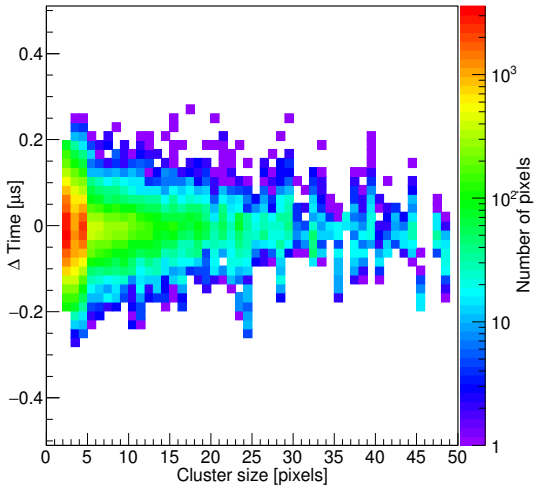

(b) Dependence between time difference of the pixels inside each cluster and the size of the cluster. In color (Z axis) is indicated the number of pixels.

Figure 11. Distribution of the time difference inside the cluster, which is defined as the region of the neighbour fired pixels. H8 beam line data in ToA mode with 48 MHz clock.

compare to the standard cluster analysis algorithm. Figure 12 shows the comparison between the results of the standard and improved cluster analysis done for the H8 beam line.

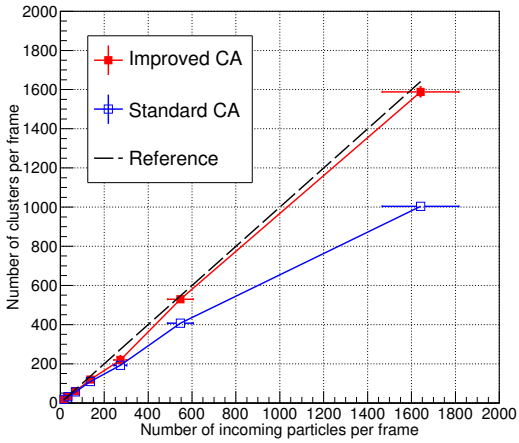

Figure 12. Comparison between two types of the Cluster Analysis (CA) for the H8 beam in ToA mode operation. The reference number of the incoming particles was taken with a plastic scintillator installed on the beam.

Figure 13 shows the distribution of the cluster size, which corresponds to the crossing particle. Assuming that the sensors are normal to the beam axis direction, one particle in most of the cases should hit only one pixel. However, due to the charge sharing between pixels, different particle

2019 JINST 14 P03018

angular distribution (see section 4) at the detector position and the orientation of the sensors with respect to the beam axis direction a significant number of clusters has more than 1 pixel size.

To obtain the calibration parameters for each sensor on the beam line it is necessary to find the most probable number of fired pixels per cluster (figure 13). The received values are ~1.8 pixels per particle for H8 beam line and ~1.7 pixels per particle for SPS.

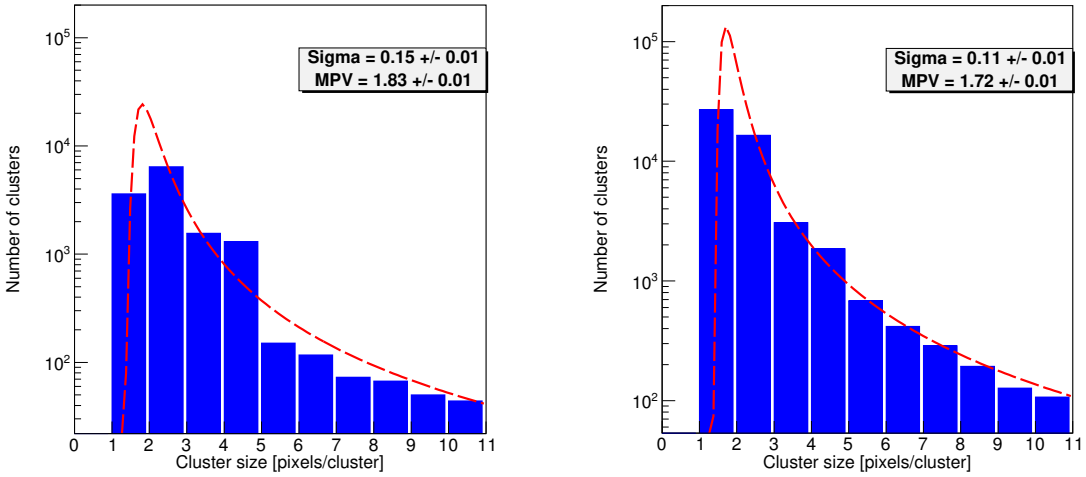

(a) H8 test beam with pions 180 GeV/c.

(b) MD at SPS with protons 270 GeV/c.

Figure 13. Distribution of the fired pixels number per cluster. The fit was done with a Landau function (red dashed line). MPV is the most probable value.

From figure 14 we can easily receive the most probable number of particles (separable clusters) per frame which is: (a) the number of particles in the primary beam at H8 beam line and (b) the number of deflected particles by the bent crystal at SPS. The measured distribution is not symmetric due to the long tail. A good fit ($\chi^2/NDF \simeq 1$) is obtained with the Vavilov distribution function [17] for figure 14a and Landau distribution function for figure 14b.

The most probable values (MPV) are: 12 particles per frame (246 μs) for H8, which means 0.5 particles per 10 μs, and 39 particles per frame (246 μs) for the SPS beam deflected by the crystal, which means 3.6 particles per machine period (~23 μs). These values are in an agreement with our expectation: 0.1–1 particle per 10 μs for H8 and few particles per period for SPS.

To measure the flux of the particles with higher statistics the devices can be used in the Medipix mode. Calculating the total number of hits in the frame divided by the calibration value (number of the fired pixels per particle) the flux of the particles for H8 (figure 15a) is about $0.6{\cdot}10^5$ pions/s (231 pions/(s·mm^2) in the beam core) and for SPS (figure 15b) is about $1.5{\cdot}10^5$ protons/s (4402 protons/(s·mm^2) in the beam core) for the active are of the Timepix sensor of 196 mm^2.

2019 JINST 14 P03018

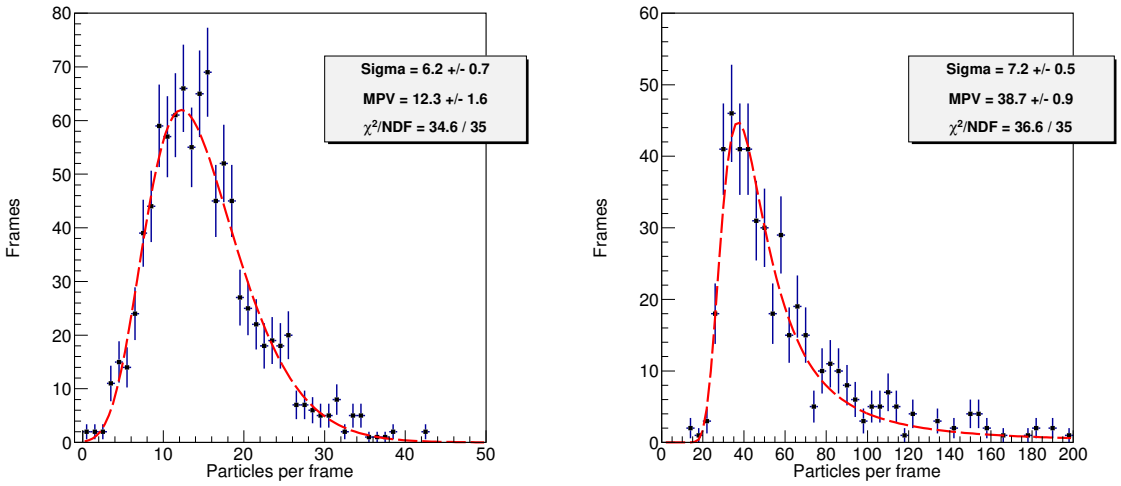

(a) H8 test beam with pions 180 GeV/c.

(b) MD at SPS with protons 270 GeV/c.

Figure 14. Number of particles per frame of 246 μs with 48 MHz in ToA mode. The fit (red dashed line) was done with the Vavilov (a) and Landau (b) distribution functions.

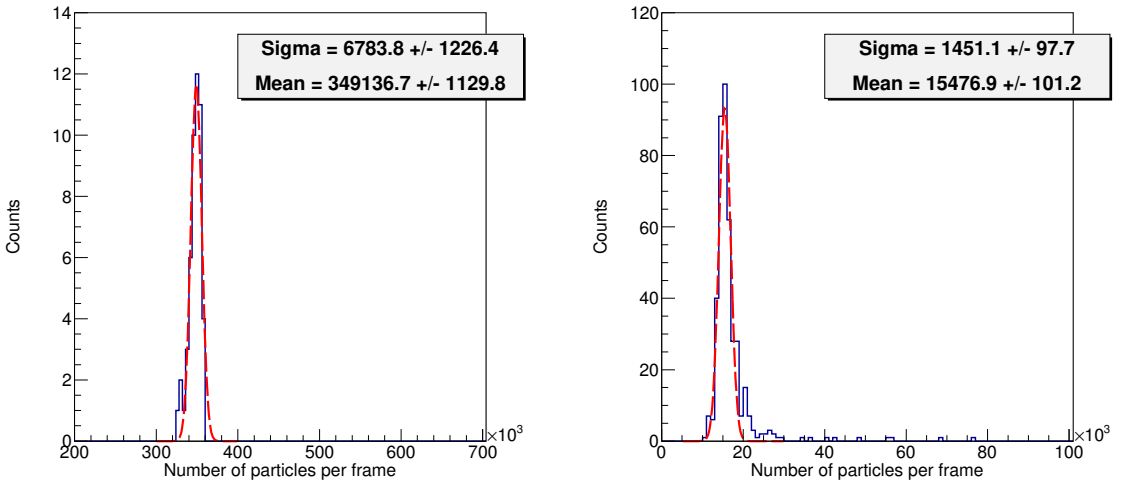

(a) H8 test beam with pions 180 GeV/c for acquisition frame of 6 s.

(b) MD at SPS with protons 270 GeV/c for acquisition frame of 0.1 s.

Figure 15. Number of particles per frame with 48 MHz clock in Medipix mode. The fit (red dashed line) was done with the Gaussian distribution functions.

2019 JINST 14 P03018

7 Timepix telescope

The measurements of the crystal parameters, such as deflection efficiency, inelastic nuclear interaction probability, are very important for the future bent crystal applications and need the track reconstruction. Thus, in April 2018 we decided to construct a short range (1.2 m long) tracker system based on 2 Timepix and 2 Quadpix (Timepix with the 4 times bigger sensitive area with 512×512 pixels) sensors to be compared with the main CMS-like tracker system. The idea to use the Timepix detector as a sensor for the particle telescope is not new [18, 19], but in the current paper we would like to describe performances of our system. Figure 16 shows the experimental layout which has been installed at the H8 beam line in April 2018. The system was placed on the motorized translation stage which gave a possibility to align the telescope with respect to the particle beam.

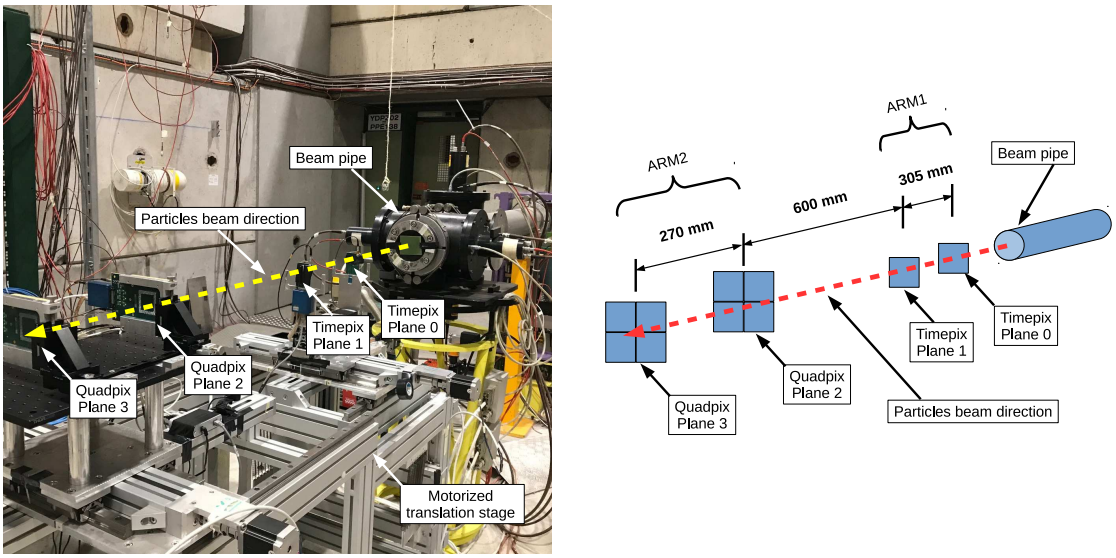

(a) The photo of the setup.

(b) The principal scheme of the setup.

Figure 16. Experimental layout of the Timepix telescope at H8.

7.1 Triggering and synchronization

A plastic scintillator placed on the beam line was used as a trigger. The scintillator gave a signal per each crossing particle. The maximum DAQ rate of the system, which consists of 4 detectors, driven by the Python script, is about 2 Hz (2 acquisition frames per second for each detector) or 500 ms of the time delay between two consecutive frames, that can be improved for the future. In order to be sure that all detectors are starting from the same trigger signal and that they are all ready to collect the data a delay of 1 s between two trigger signals was applied. Once all Timepixes are configured, we send a command simultaneously to all detector to be ready for the acquisition and wait for the arriving of the trigger signal. In such a way we provide the time synchronization between detectors. To estimate the order of the synchronization we calculate the time difference between clusters from different sensors for the same frame, taking one of them as reference (e.g. the Timepix at the Plane 1 (see figure 16)). Figure 17 shows the typically distribution of the time delay between detectors in

2019 JINST 14 P03018

ToA mode with 48 MHz clock. Taking into account the mean value of each histogram, one can see that the time shift between Plane 1 and Plane 0 is ~7.7 ns (figure 17a), between Plane 1 and Plane 2 is ~30.2 ns (figure 17b), between Plane 1 and Plane 3 is ~20.7 ns (figure 17c). Thus, we can define that the synchronization between all 4 detectors is within 2 internal clocks for 48 MHz (~20.83 ns).

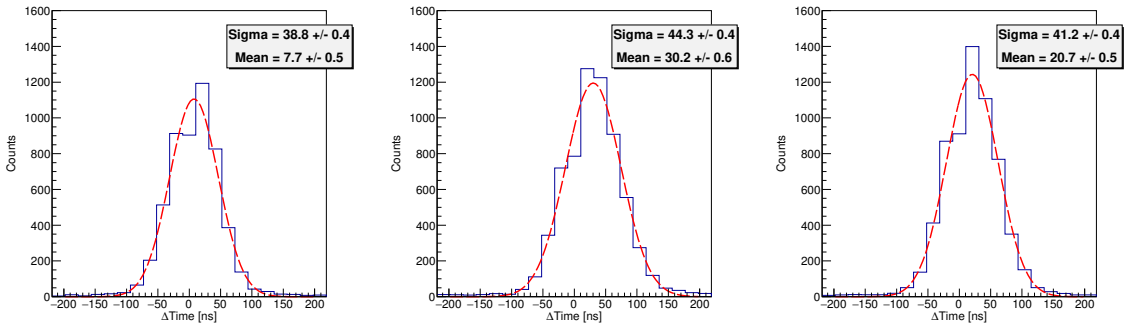

(a) Time difference between Plane 1 and Plane 0.

(b) Time difference between Plane 1 and Plane 2.

(c) Time difference between Plane 1 and Plane 3.

Figure 17. Time synchronization between 4 detectors. H8 beam line data with Timepixes in ToA mode and 48 MHz clock.

7.2 Alignment

A software alignment procedure based on particle tracks is used to calculate misalignments between sensors. In such a way the position of the hits on each plane can be corrected. The (x,y) origin of the system was placed in the center of the beam spot. Fitting the track with the straight line we can calculate the residual (difference between a hit position and interpolated position on the plane from the fit) of each sensor, taking into account the standard deviation in each pixel as σ_p=p/$\sqrt{12}$, where p means a pitch of the pixels (0.055 mm). Iterative position corrections are made in order to center the distribution of the residuals around zero (figure 18). To eliminate the rotational misalignment of the sensors around the axis of the beam direction (Z axis) we use the correlation between the residual position in X axis and interpolated impact position in Y axis for each plane.

Table 1 represents the iterative residual standard deviation (σ_r) and the twist angle (ϕ_{twist}) of each plane.

Table 1. Standard deviation of the residual distribution (σ_r) in the plane transverse to the beam direction, the twist angle (ϕ_{twist}) around Z axis of the tracker planes and the estimated resolution of each detector (σ_d).

	Axis	Plane 0	Plane 1	Plane 2	Plane 3
σ_r [μm]	X	17.3	12.5	13.8	12.9
	Y	6.6	8.5	7.9	7.0
ϕ_{twist} [μrad]	Z	-141±85	-14±106	69±139	23±100
σ_d [μm]	X	17.7	12.5	13.8	13.3
	Y	7.3	8.5	7.9	7.9

2019 JINST 14 P03018

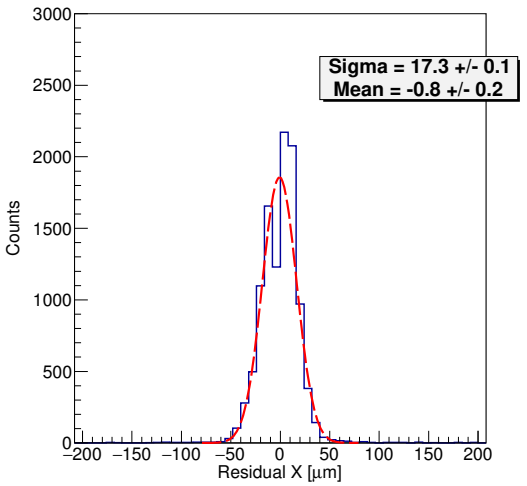

(a) Residual distribution in X direction for Plane 0 and the fitted Gaussian (red dashed line).

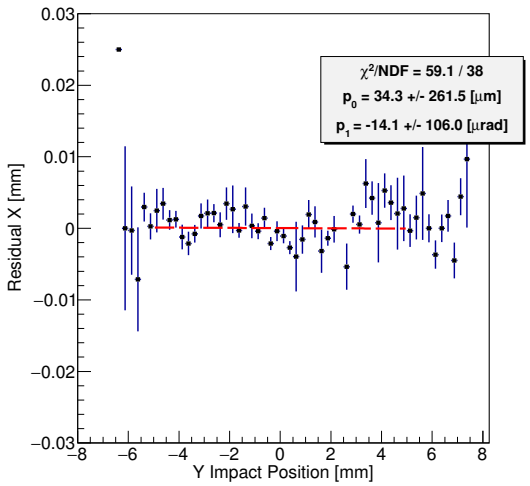

(b) The mean value of the residual in X axis as a function of the estimated impact position in Y axis for Plane 1. The fit (red dashed line) is done using the first order polynomial function: $f(x) = p_1 x^1 + p_0$.

Figure 18. Spatial alignment characteristics of the telescope.

7.3 Tracks reconstruction

After the procedure of the spatial alignment of the system described above we performed the reconstruction of the particles tracks based on the algorithm which is close to one described in [11].

We may assume that in the future the crystal under investigation will be placed between Plane 1 and Plane 2, 300 mm from each plane. It means that the upstream section of the tracker (Arm 1), which consists of the Plane 0 and Plane 1, measures the incoming particles tracks, at the same time the outgoing tracks are measured using the downstream section (Arm 2), which is made of Plane 2 and Plane 3. To measure the error of the system in this configuration we have to take into account the not negligible scattering in the sensor and its resolution.

The estimated detectors resolution was calculated as $\sigma_d = \sqrt{\sigma_r^2 + \sigma_f^2}$, where σ_r is determined from the residual distribution, σ_f includes the errors due to the scattering as described in [20]. The results can be found in table 1. According to [18] each plane contributes 300 μm thick silicon sensor, a Timepix chip (700 μm thick) and a PCB with 100 μm of copper and 1.3 mm of FR4, the angular error per plane due to the scattering is ~10.5 μrad for a 180 GeV/c pion beam. The spatial resolution of the detectors is very close to the digital resolution of $\sigma_p = 15.88$ μm.

The main parameters of the track reconstruction (figure 19) are θ_{in} (incoming angle), θ_{out} (outgoing angle) and d_0 (impact parameter at the crystal position).

Figure 20 shows the angular resolution of the telescope for both horizontal and vertical projections, measured as the angular deviation between incoming and outgoing tracks, reconstructed by the upstream (ARM1) and downstream (ARM2) arms of the system. Only single track events were taken into account. The measured angular resolution (Sigma) is around 73 μrad in X and Y axes and the angular misalignment (Mean) between two arms of the telescope is around 30 μrad

2019 JINST 14 P03018

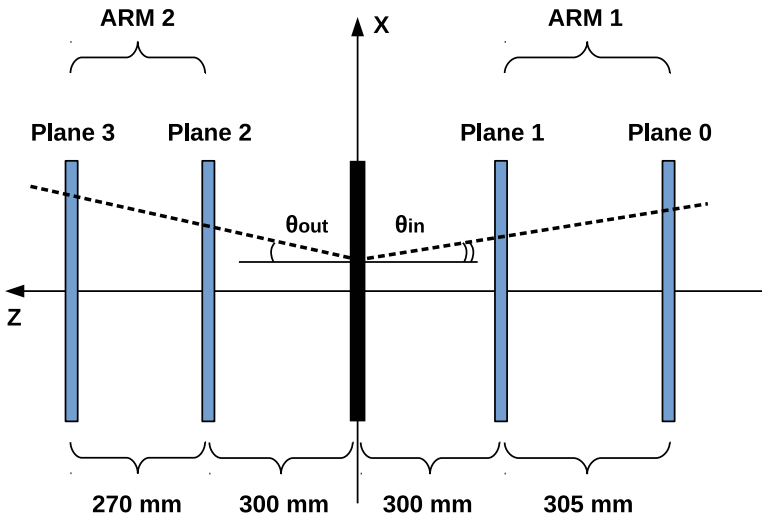

Figure 19. Track reconstruction scheme. θ_{in} and θ_{out} are incoming and outgoing angles respectively at the possible crystal position (black rectangle).

and 4 μrad in horizontal and vertical planes respectively. The increasing of the telescope length can linearly decrease the value of the angular resolution.

To estimate the track reconstruction efficiency we can use the amount of the reconstructed tracks, number of recorded frames and DAQ rate (can be improved). Taking into account the flux of the particles ($\sim 10^5$ p/s), the calculated value of the efficiency is around 10 % of the total incoming particles.

8 Conclusion

The Timepix detector is a device, which completely fulfilled UA9 requirements for the quantified beam monitoring on the beam line and in a secondary vacuum inside a beam pipe (three years of operation with about 0.4 kGy/y radiation dose) of the accelerator machine like the SPS at CERN. For the first time, it was measured at SPS the flux of the deflected halo particles by the bent silicon crystal. Operation in a ToA mode gives a possibility to follow the beam evolution turn per turn for the main beam instabilities in time.

A sequence of several Timepix detectors has a performance, which is good and comparable with a more sophisticated silicon microstrip telescope of UA9 at H8 beam line. The average spatial resolution is less than 20 μm per sensor. The telescope provides very good 70 μrad angular resolution for reconstructed particle tracks with a flight base of 1.2 m and track reconstruction efficiency of about 24 % (with a triggering rate of about 1 Hz). The increase of the flight base (up to 10–20 m),

2019 JINST 14 P03018

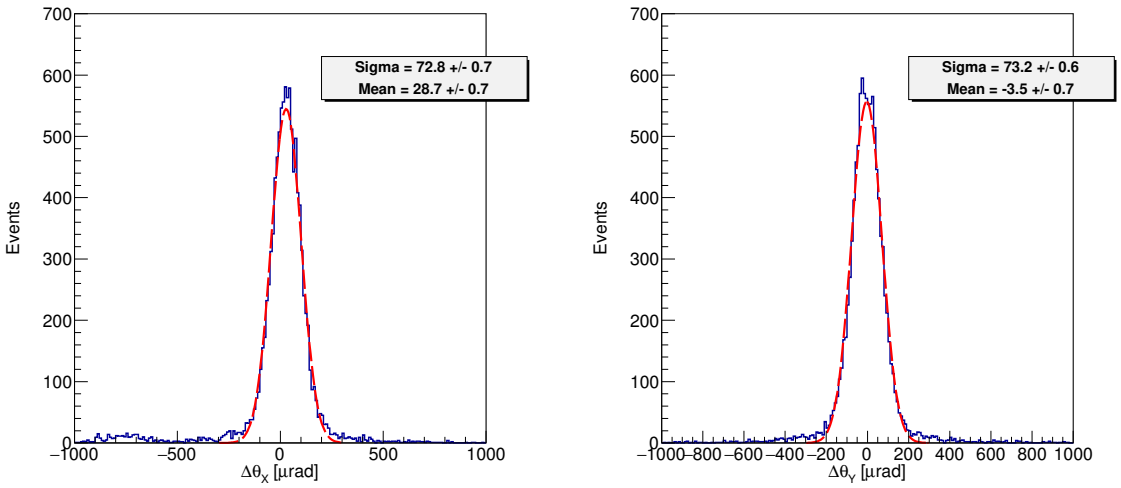

(a) In horizontal axis.

(b) In vertical axis.

Figure 20. Angular resolution ($\Delta\theta = \theta_{\text{out}} - \theta_{\text{in}}$) of the telescope in the plane transverse to the beam direction. The fit (red dashed line) was done with the Gaussian function.

can give a possibility to improve the angular resolution of the system up to the physical limitation of 10.5 μrad, which is related to the multiple scattering inside each sensor. The system is portable and can be installed on the different beam lines for crystal measurements and characterization.

Acknowledgments

The authors are grateful to other members of the UA9 collaboration for their support and their contribution to the development of the experimental apparatus used in this study. This research was partially conducted in the scope of the IDEATE International Associated Laboratory (LIA). We would like to thank Erik Heijne for his helpful advices in the preparation of this paper, Luca Foggetta and Claudio Di Giulio for the studies on the DAQ synchronization. The authors warmly acknowledge the support of Michael Campbell from the Medipix collaboration for the readout electronics.

References

[1] V. Biryukov, Y. Chesnokov and V. Kotov, *Crystal channeling and its application at high energy accelerators*, Springer, Germany (1997).

[2] V. Puill et al., *The CpFM, an in-vacuum Cherenkov beam monitor for UA9 at SPS*, 2017 *JINST* **12** P04029.

[3] X. Llopart, R. Ballabriga, M. Campbell, L. Tlustos and W. Wong, *Timepix, a 65k programmable pixel readout chip for arrival time, energy and/or photon counting measurements*, *Nucl. Instrum. Meth.* **A 581** (2007) 485 [*Erratum ibid.* **A 585** (2008) 106].

[4] M. Campbell, 10 *years of the Medipix2 collaboration*, *Nucl. Instrum. Meth.* **A 633** (2011) S1.

2019 JINST 14 P03018

[5] M. Kroupa, J. Jakubek and F. Krejci, *Charge collection characterization with semiconductor pixel detector Timepix*, *IEEE Nucl. Sci. Symp. Conf. Rec.* (2008) 259.

[6] D.H. Wilkinson, *The Geiger discharge*, *Phys. Rev.* **74** (1948) 1417.

[7] R. Ballabriga, M. Campbell and X. Llopart, *ASIC developments for radiation imaging applications: the Medipix and Timepix family*, *Nucl. Instrum. Meth.* **A 878** (2018) 10.

[8] V. Kraus, M. Holik, J. Jakubek, M. Kroupa, P. Soukup and Z. Vykydal, *FITPix: fast interface for Timepix pixel detectors*, 2011 *JINST* **6** C01079.

[9] D. Turecek, T. Holy, J. Jakubek, S. Pospisil and Z. Vykydal, *Pixelman: a multi-platform data acquisition and processing software package for Medipix2, Timepix and Medipix3 detectors*, 2011 *JINST* **6** C01046.

[10] E.Jr. Schioppa, *Energy calibration procedure of a pixel detector*, notes. draft Ph.D. thesis, NIKHEF, The Netherlands (2013).

[11] M. Pesaresi et al., *Design and performance of a high rate, high angular resolution beam telescope used for crystal channeling studies*, 2011 *JINST* **6** P04006.

[12] W. Scandale et al., *Apparatus to study crystal channeling and volume reflection phenomena at the SPS H8 beamline*, *Rev. Sci. Instrum.* **79** (2008) 023303.

[13] W. Scandale et al., *The UA9 experimental layout*, 2011 *JINST* **6** T10002 [arXiv:1106.5861].

[14] R. Losito, *UA9 instrumentation and detectors in the CERN-SPS*, in *Proceedings of IPAC'*10, Kyoto, Japan (2010), pg. 1692.

[15] P. Russo et al., 18*F-FDG positron autoradiography with a particle counting silicon pixel detector*, *Phys. Med. Biol.* **53** (2008) 6227.

[16] C. Scharf and R. Klanner, *Precision measurement of the carrier drift velocities in* ⟨100⟩ *silicon*, 2015 *JINST* **10** C11008 [arXiv:1509.04183].

[17] M.M. Devi et al., *Hadron energy response of the iron calorimeter detector at the India-based neutrino observatory*, 2013 *JINST* **8** P11003 [arXiv:1304.5115].

[18] K. Akiba et al., *The Timepix telescope for high performance particle tracking*, *Nucl. Instrum. Meth.* **A 723** (2013) 47 [arXiv:1304.5175].

[19] S.P. George, F. Murtas, J. Alozy, A. Curioni, A.B. Rosenfeld and M. Silari, *Particle tracking with a Timepix based triple GEM detector*, 2015 *JINST* **10** P11003.

[20] M. Pentia, G. Iorgovan and A. Mihul, *Multiple scattering error propagation in particle track reconstruction*, *Rom. J. Phys.* **40** (1995) 181 [hep-ex/9406006].

2019 JINST 14 P03018